Optimal Periodic Variable Switching PWM for Harmonic Performance Enhancement in Grid-Connected Voltage Source Converters

Wu, Yang; Xu, Junzhong; Soeiro, Thiago B.; Stecca, Marco; Bauer, Pavol

DOI
10.1109/TPEL.2022.3141268

Publication date
2022

Document Version
Accepted author manuscript

Published in
IEEE Transactions on Power Electronics

This article has been accepted for publication in a future issue of this journal, but has not been fully edited. Content may change prior to final publication. Citation information: DOI 10.1109/TPEL.2022.3141268, IEEE Transactions on Power Electronics

Optimal Periodic Variable Switching PWM for Harmonic Performance Enhancement in Grid-Connected Voltage Source Converters

Yang Wu, *Student Member, IEEE*, Junzhong Xu, *Member, IEEE*, Thiago Batista Soeiro, *Senior Member, IEEE*, Marco Stecca, *Student Member, IEEE*, and Pavol Bauer, *Senior Member, IEEE*

***Abstract*—Variable switching frequency PWM (VSFPWM) modulation can be advantageously implemented in industrial applications such as renewable energy, motor drives, and Uninterrupted Power Supply systems UPS, etc., to reduce the injected current harmonic amplitudes, to suppress audible noise, and to improve semiconductor power efficiency. In this work, the usage of periodic VSFPWM methods in a voltage source converter (VSC) is proposed, analyzed and benchmarked in terms of harmonic spectrum spreading, following the IEEE-519 current harmonic standard for the connection to the distribution grid. Particular attention is paid to the influence of VSFPWM on the AC filter design. Firstly, the analytical model of the voltage harmonic spectrum generated by a three-phase three-wire two-level VSC implementing several periodic VSFPWM methods are derived. Subsequently, a design guideline for the commonly used LCL filter in the grid-tied VSC application is proposed which minimizes the size requirement of the necessary components. The voltage spectrum models of the proposed VSFPWM method and the optimal switching profiles are verified by Matlab/Simulink simulations and a 5kW three-phase two level VSC hardware demonstrator. The study shows that the AC filter power density for the studied VSFPWM methods can be greatly increased when compared to the conventional and widely employed constant switching frequency continuous PWM strategies.**

***Index Terms*—Variable switching frequency PWM (VSF-PWM), filter design, spectrum model, optimal design.**

NOMENCLATURE

$i_{\rm c}$, $i_{\rm g}$	Converter-/grid-side phase current
$V_{\rm ac}$,$v_{\rm ac}$	AC source (grid) phase voltage
$V_{\rm c}$, $v_{\rm c}$	Converter output phase voltage
$V_{\rm dc}$	DC bus voltage
M	Modulation depth
$J_{\rm n}(x)$	Bessel function of the first kind
$L_{\rm c}$, $L_{\rm g}$, $L_{\rm T}$	Converter-/grid-side/total inductance
$L_{\rm T}$	LCL filter total inductance
$C_{\rm f}$	LCL filter capacitance
$\omega_{\rm c}$, $\omega_{\rm o}$, $f_{\rm c}$, $f_{\rm o}$	Carrier and reference frequency
$\theta_{\rm c}$, $\theta_{\rm o}$	Phase of carrier and reference signal
$f_{\rm c0}$	Centered switching(carrier) frequency
$f_{\rm res}$	LCL filter resonance frequency
$f_{\rm m}$	Frequency of periodc switching profile
$\omega_{\rm b}$, $f_{\rm b}$	Switching frequency variation band
$\omega_{\rm crit}$, $f_{\rm crit}$	Critical harmonic frequency
$V_{\rm crit}$, $I_{\rm crit}$, $f_{\rm crit}$	Critical harmonic voltage / current

Manuscript received August 12, 2021; revised October 04, 2021; accepted December 31, 2021. This research has been funded within the Power2Power project, which is a European co-funded innovation project on Semiconductor Industry. The project receives grants from the European H2020 research and innovation program, ECSEL Joint Undertaking, and National Funding Authorities from eight involved countries under grant agreement No. 826417. The participating countries are Austria, Finland, Germany including the Free States of Saxony and Thuringia, Hungary, the Netherlands, Slovakia, Spain and Switzerland. (*Corresponding author: Junzhong Xu.*)

Yang Wu, Thiago Batista Soeiro, Marco Stecca and Pavol Bauer are with the Department of Electrical Sustainable Energy, DCE&S group, Delft University of Technology, 2628 CD Delft, South Holland, The Netherlands (e-mail: y.wu-6@tudelft.nl, t.batistasoeiro@tudelft.nl, M.Stecca@tudelft.nl, p.bauer@tudelft.nl).

Junzhong Xu is with the Department of Electrical Engineering, Shanghai Jiao Tong University, Shanghai 200240, China, and also with the Key Laboratory of Control of Power Transmission and Conversion, Ministry of Education, Shanghai 200240, China (e-mail: junzhongxu@sjtu.edu.cn).

I. INTRODUCTION

DUE to the rapid development of renewable technology and wider adoption of electric vehicles, the pursuit of compact and efficient grid-tied power electronic converters are becoming increasingly important for photovoltaic and wind power generation, and battery fast charging stations. Pulse-width-modulation (PWM) based voltage source converters (VSCs) are widely employed as grid-tied converters because of their robustness and simplicity [1]. Correspondingly, LCL filters are adopted to mitigate the current harmonics generated by the PWM based VSCs. Typically, the LCL filter is one of the bulkiest and heaviest part in the high power converter system. Hence, considerable research efforts in physical design and circuit topology have been devoted aiming at reducing the filter size and weight. It is recognizable that the design of a smaller inductor is possible if the application requirements can be fullfilled with the need of less magnetic energy storage, e.g. by reducing the need of inductance value [2], [3]. Conventional approaches for reducing the harmonic generated by the VSC, and therefore the required filtering inductance, consists on increasing the switching frequency, adopting interleaved or multi-level converter topologies, and implementing specific modulations [4]–[9].

Variable switching frequency PWM (VSFPWM), for instance, is an interesting strategy to be implemented in VSCs because of its effectiveness in improving the switching loss, current ripple, EMI, and above all its simple digital implementation [10]–[15]. More importantly, the spread spectrum caused by VSFPWM can also benefit the filter design for the

This article has been accepted for publication in a future issue of this journal, but has not been fully edited. Content may change prior to final publication. Citation information: DOI 10.1109/TPEL.2022.3141268, IEEE Transactions on Power Electronics

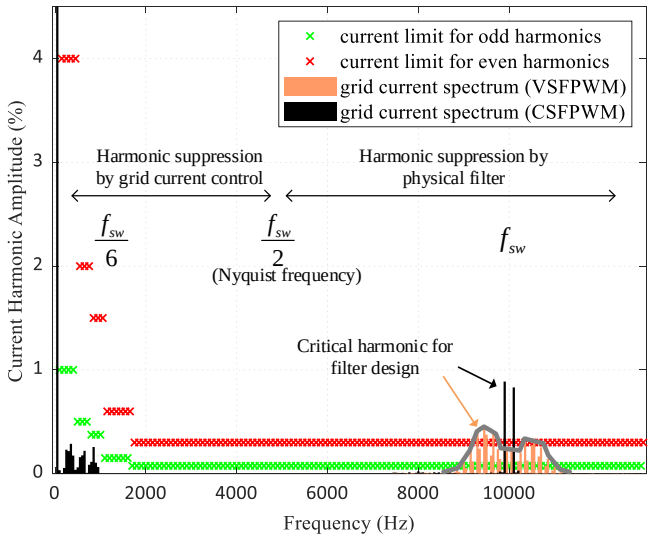

Fig. 1. IEEE-519 harmonic current standard and typical grid current harmonic spectrum with CSFPWM and VSFPWM.

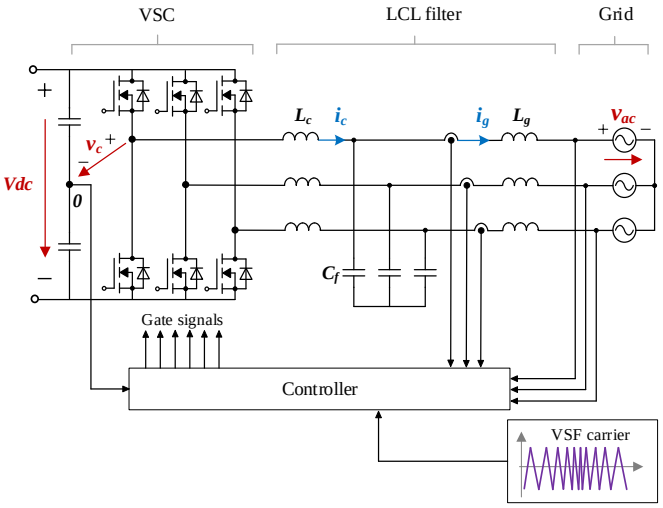

Fig. 2. Grid-tied VSC with LCL filter adopting VSFPWM.

VSC. However, there is lack of research efforts about this concept at present. The filter used for grid-tied converter must be well-designed to comply with the grid connection standard, in particularly the harmonic current standards such as IEEE-519-2014 [4]. As presented in Fig. 1, the VSFPWM method spreads out the converter output voltage spectrum, thus giving a similarly wide harmonic spectrum with lower amplitudes for the grid current compared with the normally adopted constant switching frequency PWM (CSFPWM), when an AC filter is applied. The magnitude of the critical harmonic for the filter design is significantly reduced by VSFPWM. In other words, the filtering requirement can be alternatively lowered with the VSFPWM while maintaining the same level of critical current harmonic presented by the CSFPWM. Therefore the compact design of the LCL filter can be realized by the VSFPWM, leading to lower loss and weight in the filter, which can consequently improve the system efficiency and power density.

VSFPWM strategies can be categorized into two types: random (or chaotic) and periodic switching frequency profiles. From the perspective of shaping the spectra of the PWM output voltage for filter design, the periodic patterns are preferred, since random profiles do not provide a tight control on the spectrum band [16]–[18]. The critical harmonic for the filter design is found to be closely correlated with the band of the spectrum induced by the periodic VSFPWM. Hence, the LCL filter can be designed in consideration of not only normal design criteria but also the profile of the periodic VSFPWM. Such a design requires the accurate voltage spectrum model of the three phase PWM converter. The work in [17], [18] firstly studied the band of the spectrum induced by the periodic switching frequency profile in a PWM converter but did not provide further description of the spectrum contents. In [19], the spectrum model was presented in complex domain for DC/DC PWM converters with the consideration of the sinusoidal switching profile only. Recently, [16] derived the analytical spectrum model for three phase PWM converter based on the PWM output voltage expressions described by [20]. However, the derived model only applies to sinusoidal switching profile and is not valid for generic periodic switching profiles which includes several harmonics instead of a single sinusoid.

The research on the LCL filter design with VSFPWM is very limited in the literature. Only the restraint of current ripple on the filter inductance [21], [22] or the basic requirement asscociated with the LCL filter resonance are considered [4], [23]. By contrast, this paper investigates the influence of the VSFPWM following periodic switching frequency profiles on the design of the LCL filter of a three-phase three-wire two-level VSC which complies to the grid harmonic IEEE-519-2014 standard, illustrated in Fig.1. The changing frequency profiles considered here are based on conventional waveform shapes, i.e., triangle and sinusoidal waveforms [17]–[19], due to their simple implementation in microcontrollers and straight-forward identification of the critical current harmonic for the AC filter design. Therefore, the optimal periodic VSFPWM profile is identified in this paper and a guideline for the LCL filter design is proposed which maximizes the VSC power density.

The research contributions of this paper are:

1) The derivation of the PWM converter voltage spectrum model for the generic periodic VSFPWM profiles.
2) A straight-forward design guideline for the LCL filter of a grid-tied VSC implementing a periodic VSFPWM profile which substantially reduce the AC filter requirement while maintaining the current THD and power efficiency which are achieved by the equivalent CSFPWM strategy.
3) The benchmaking and insights gained on the attained LCL filter performance in harmonic attenuation for grid compliance for several periodic profile VSFPWM and standard CSFPWM strategies.

This paper is organized as follows. Section II presents the derivation of the time-domain model of the two-level VSC output voltage. Section III describes the design guidelines of the optimal periodic VSFPWM profile. Finally, Section IV discusses the simulation and experimental results verifying the developed analytical models and proposed LCL filter design.

This article has been accepted for publication in a future issue of this journal, but has not been fully edited. Content may change prior to final publication. Citation information: DOI 10.1109/TPEL.2022.3141268, IEEE Transactions on Power Electronics

$$V_c(x,y) = \frac{A_{00}}{2} + \underbrace{\sum_{n=1}^{\infty}(A_{0n}\cos ny + B_{0n}\sin ny)}_{\text{Fundemental Component \& Baseband Harmonics}} + \underbrace{\sum_{m=1}^{\infty}(A_{m0}\cos mx + B_{m0}\sin mx)}_{\text{Carrier Harmonics}} + \underbrace{\sum_{m=1}^{\infty}\sum_{\substack{n=-\infty \\ n\neq 0}}^{\infty}[A_{mn}\cos(mx+ny) + B_{mn}sin(mx+ny)]}_{\text{Sideband Harmonics}} \tag{1}$$

$$\begin{aligned} V_{\mathrm{c}}(t) =& \frac{2V_{\mathrm{dc}}}{\pi}\sum_{n=1}^{\infty}\frac{J_{\mathrm{n}}(n\frac{\omega_{\mathrm{o}}}{\omega_{\mathrm{c}}}\frac{\pi}{2}M)}{(n\frac{\omega_{\mathrm{o}}}{\omega_{\mathrm{c}}})}\sin[n(1+\frac{\omega_{\mathrm{o}}}{\omega_{\mathrm{c}}})\frac{\pi}{2}]\cos n(\omega_{\mathrm{o}}t+\theta_{\mathrm{o}}) + \frac{2V_{\mathrm{dc}}}{\pi}\sum_{m=1}^{\infty}\frac{J_0(m\frac{\pi}{2}M)}{m}\sin(m\frac{\pi}{2})\cos[m(\omega_{\mathrm{c}}t+\theta_{\mathrm{c}})] + \\ & \frac{2V_{\mathrm{dc}}}{\pi}\sum_{m=1}^{\infty}\sum_{\substack{n=-\infty \\ n\neq 0}}^{\infty}\frac{J_{\mathrm{n}}[(m+n\frac{\omega_{\mathrm{o}}}{\omega_{\mathrm{c}}})\frac{\pi M}{2}]}{m+n\frac{\omega_{\mathrm{o}}}{\omega_{\mathrm{c}}}}\sin[(m+n\frac{\omega_{\mathrm{o}}}{\omega_{\mathrm{c}}}+n)\frac{\pi}{2}]\cos[m(\omega_{\mathrm{c}}t+\theta_{\mathrm{c}})+n(\omega_{\mathrm{o}}t+\theta_{\mathrm{o}})] \\ =& \Re(\sum_{m=0}^{\infty}\sum_{n=-\infty}^{\infty}A_{\mathrm{mn}}\cdot e^{\mathrm{j(m(\omega_c t+\theta_c)+n(\omega_o t+\theta_o)))}}) = \Re(\sum_{m=0}^{\infty}\sum_{n=-\infty}^{\infty}A_{mn}\cdot e^{\mathrm{j(mx+ny)}}) \end{aligned} \tag{2}$$

II. Converter Voltage Spectrum Model

A. Spectrum Model for CSFPWM

To simplify the analysis and model derivations, the Sinusoidal-PWM (SPWM) is presented in this section. These mathematical derivations built based on the SPWM can be extended to other continuous PWM methods, e.g., THIPWM and SVPWM [20], [24], [25], which are preferably implemented in practical systems because of their higher DC bus voltage utilization. As depicted in Fig. 2, the converter output phase voltage V_{c} of the three-phase two-level converter is determined by the switching states of the semiconductor devices, which are directed by the intersections between the sinusoidal reference and triangular carrier signals, as illustrated in Fig. 3. According to the double Fourier analysis (DFA) [20], the output phase voltage $V_c(x,y)$ is the function of two independent variables as expressed by (1). In (1), m and n are multiples of the carrier and reference signal frequencies while A_{mn} and B_{mn} are the resultant coefficients of the DFA. The first term A_{00} shown in (1) represents the DC offset, which is zero for the converter circuit shown in Fig. 2. The first summation term is the base-band harmonic components and the second summation term represents the carrier harmonic components. The last one represents the side-band harmonic components. The two variables x and y represent the phases of the carrier and reference signals under the constant carrier frequency modulation respectively, which are expressed as:

$$\begin{cases} x(t) = \omega_c t + \theta_c \\ y(t) = \omega_o t + \theta_o \end{cases} \tag{3}$$

where ω_c and ω_o are the angular frequencies for the carrier and reference signals (switching and fundamental frequencies) respectively, and θ_c and θ_o are the phases for the carrier and reference signals. The VSC output voltage with CSFPWM under the symmetrical regular sampling can be generally

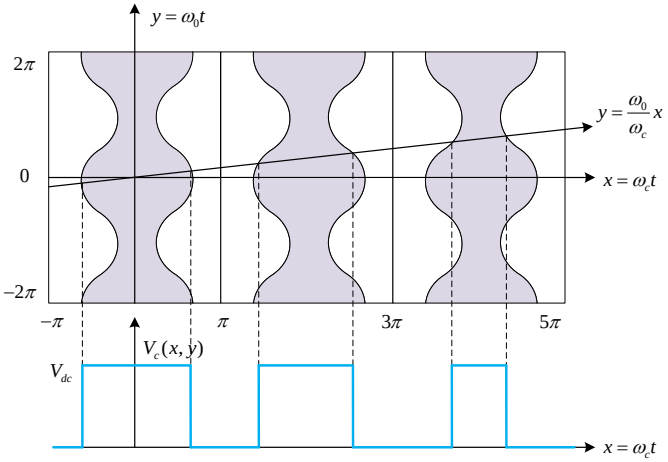

Fig. 3. Triangular carrier-based CSFPWM (natural sampling).

expressed as (2) in time domain, with the complex-form coefficients derived by using the double-integral:

$$\begin{aligned} C_{\mathrm{mn}} &= A_{\mathrm{mn}} + jB_{\mathrm{mn}} \\ &= \frac{1}{2\pi^2}\int_{-\pi}^{\pi}\int_{-\pi}^{\pi}V_c(x,y)e^{j(mx+ny)}\mathrm{d}x\mathrm{d}y \end{aligned} \tag{4}$$

Therein $J_{\mathrm{n}}(x)$ is the Bessel function of the first kind, and M is the modulation depth. M is defined as $2V_{\mathrm{ac}}/V_{\mathrm{dc}}$ and V_{ac} and V_{dc} are the magnitude of the AC phase voltage and DC bus voltage respectively [20].

B. Spectrum Model for Periodic VSFPWM

When periodic VSFPWM is applied, the phases of the two signals are modified as:

$$\begin{cases} x(t) = \int_0^t \omega_{\mathrm{c}}(\tau)\mathrm{d}\tau + \theta_{\mathrm{c}} \\ y(t) = \omega_{\mathrm{o}}t + \theta_{\mathrm{o}} \end{cases} \tag{5}$$

This article has been accepted for publication in a future issue of this journal, but has not been fully edited. Content may change prior to final publication. Citation information: DOI 10.1109/TPEL.2022.3141268, IEEE Transactions on Power Electronics

The spectrum model, hence becomes more complicated and very difficult to be directly derived with DFA because of the non-linearity caused by the periodic time-varying variable $\omega_{\rm c}(t)$ appearing in the carrier angular frequency $x(t)$. Tripple Fourier analysis is also not applicable since variable $x(t)$ and $\omega_{\rm c}(t)$ are inter-coupled and not linear. To derive the spectrum expression some assumptions are adopted in this work to approximate the derived voltage expression:

1) The ratio between the centered switching frequency and the fundamental frequency $\omega_{\rm c0}/\omega_{\rm o}$ should be large enough, where the centered angular frequency $\omega_{\rm c0}$ is the average of $\omega_{\rm c}(t)$ during its period.
2) The variation band of the switching frequency $\omega_{\rm b}$ (or $f_{\rm b}$), which is half of the peak-to-peak variation of the switching profile, should be relatively small compared to the centered frequency $\omega_{\rm c0}$.

These two assumptions guarantee that the influence of the varying switching frequency on the coefficients presented in (2) can be negligible and hence the forms of these coefficients remain unchanged in the following mathematical derivations, except that $\omega_{\rm c}$ is replaced by $\omega_{\rm c0}$. A generic periodic switching frequency $f_{\rm c}(t)$ can be expanded into the following Fourier series:

$$\begin{aligned} f_{\rm c}(t) &= \frac{a_0}{2} + \sum_{k=1}^{\infty} a_{\rm k}\cos(2\pi k f_{\rm m} t) + b_{\rm k}\sin(2\pi k f_{\rm m} t) \\ &= f_{\rm c0} + \sum_{k=1}^{\infty} C_k \sin(2\pi k f_{\rm m} t + \theta_{\rm k}) \end{aligned} \tag{6}$$

where f_{c0} is the centered switching frequency and f_m is the frequency of the periodic switching profile. Substituting (5) and (6) into the phasor form presented in (4), and assuming that the initial phases of the carrier and reference signals are zero ($\theta_{\rm c}$, $\theta_{\rm o}$=0), then the expression of the output voltage becomes:

$$\begin{aligned} V_c(t) =& \Re\Big(\sum_{m=0}^{\infty}\sum_{n=-\infty}^{\infty} A_{\rm mn}\cdot e^{{\rm j}2\pi({\rm m}\int_0^{\rm t} {\rm f_c}(\tau){\rm d}\tau + {\rm nf_o t})}\Big) \\ =& \Re\Big(\sum_{m=0}^{\infty}\sum_{n=-\infty}^{\infty}\{A_{mn}\cdot e^{{\rm j}(2\pi({\rm mf_{c0}+nf_o})t+\varphi_{\rm m})} \\ & \cdot \underbrace{\prod_{k=1}^{\infty} e^{-{\rm j}\frac{{\rm mC_k}}{{\rm kf_m}}\cos(2\pi {\rm kf_m t}+\theta_{\rm k})}\}}_{\text{rear term due to VSFPWM}}\Big) \end{aligned} \tag{7}$$

where

$$\varphi_{\rm m} = \sum_{k=1}^{\infty}\frac{mC_{\rm k}\cos(\theta_{\rm k})}{kf_{\rm m}} \tag{8}$$

In (7), the rear term is caused by the variation of the switching frequency. However, (7) is too complex and indirect to be used for calculation and thus requires a further simplification. By implementing Jacobi-Anger expansions [20], the expression for the output voltage can be simplified as:

$$V_c(t) = \Re\Big(\sum_{m=0}^{\infty}\sum_{n=-\infty}^{\infty}\sum_{l=-\infty}^{\infty} C_{\rm mnl}\cdot e^{{\rm j}2\pi({\rm mf_{c0}t+nf_o t+lf_m t})}\Big) \tag{9}$$

where

$$C_{\rm mnl} = A_{\rm mn}e^{{\rm j}\varphi_{\rm m}}\cdot\left\{\sum_{\sum r_k\cdot k=l}(\prod_{k=1}^{\infty} h(m,k,r_k))\right\} \tag{10}$$

$$A_{\rm mn} = \frac{2V_{\rm dc}J_{\rm n}[(m+n\frac{\omega_{\rm o}}{\omega_{\rm c0}})\frac{\pi M}{2}]}{\pi(m+n\frac{\omega_{\rm o}}{\omega_{\rm c0}})}\sin[(m+n\frac{\omega_{\rm o}}{\omega_{\rm c0}}+n)\frac{\pi}{2}] \tag{11}$$

$$h(m,k,r) = J_{\rm r}(\frac{mC_{\rm k}}{kf_{\rm m}})\cdot e^{{\rm j}({\rm r}(\theta_{\rm k}-\pi/2))} \tag{12}$$

Since the phase of the reference signal $\theta_{\rm o}$ is equal to zero, the expression (9) describes analytically the output voltage of phase A, i.e., $V_{\rm c}$ with the VSFPWM. The expressions for phase B and C can be derived accordingly by replacing $\theta_{\rm o}$ with $-2\pi/3$ and $2\pi/3$ respectively. It is noteworthy that the spectrum of the output voltage can be obtained based on (9) because of the triple summation series form, and phasor representation. It can be noted that the side-band harmonics are the resultant contributed by the integer variables n and l, which represent the side-band caused by CSFPWM and VSFPWM respectively.

It is noted that the triple summation series form presented in (9) is valid only when the aforementioned two assumptions are satisfied. The assumptions guarantee that the difference of the coefficient $A_{\rm mn}$ during the switching frequency variation is negligible and thus the coefficient can be calculated at the centered frequency $f_{\rm c0}$ as shown in (11) and remain unchanged regardless the switching frequency. The coefficient $C_{\rm mnl}$ contains the magnitude and phase information of the spectrum. However, for each possible side-band $lf_{\rm m}$ caused by VSFPWM there are infinite groups of $r_{\rm k}$ and hence the calculation of (10) becomes cumbersome. Specially, if $f_{\rm c}(t)$ varies sinusoidally with the frequency f_m, the coefficient $C_{\rm mnl}$ is reduced to:

$$C_{\rm mnl} = A_{\rm mn}J_{\rm l}(\frac{mC_1}{f_{\rm m}})\cdot e^{j(\varphi_{\rm m1}+l(\theta_1-\pi/2))} \tag{13}$$

which is simpler and more convenient to use. Although the developed analytical spectrum model is derived based on SPWM, the same derivation approach is also applicable to other modulation methods e.g, THIPWM and SVPWM. From (7), the rear term due to VSFPWM implies that the influence of the VSFPWM is decoupled from the normal CSFPWM operation. Therefore, Eq. (9), (10) and (11) still hold for other modulations while (11) should be replaced with the coefficient $A_{\rm mn}$ derived based on the CSFPWM operation according to the modulation adopted. The expression of $A_{\rm mn}$ for THIPWM and SVPWM can be found in [20], which is rather complicated and will not be presented in this paper due to space limitations.

C. DM and CM Harmonic Spectrum

In a three-phase three-wire VSC system, as the one shown in Fig. 2, due to the intrinsic high impedance for the generated zero sequence voltage components, only the differential-mode (DM) currents are considered to flow into the circuit for the spectrum of interest defined by the IEEE-519-2014 guidelines. Therefore, the circulating common-mode (CM) current

This article has been accepted for publication in a future issue of this journal, but has not been fully edited. Content may change prior to final publication. Citation information: DOI 10.1109/TPEL.2022.3141268, IEEE Transactions on Power Electronics

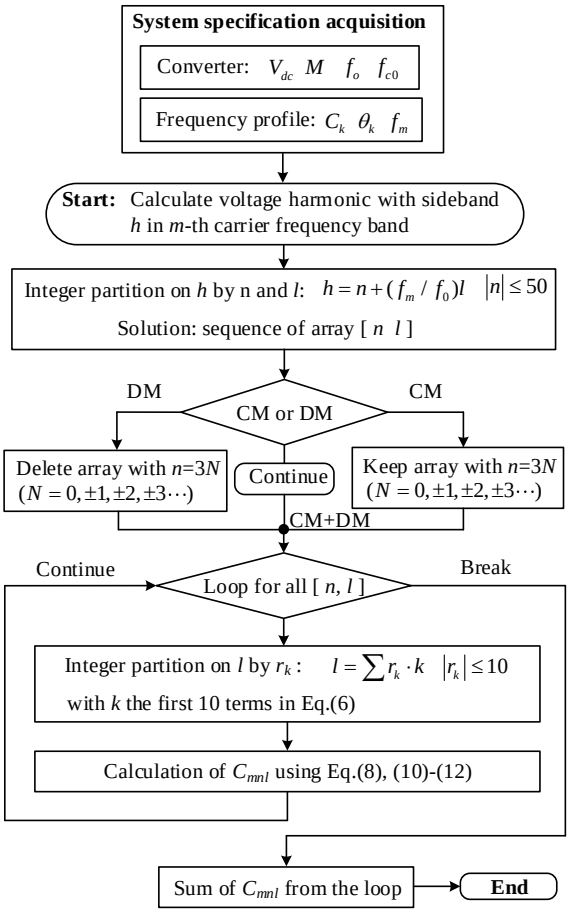

Fig. 4. Calculation algorithm of the VSC generated voltage spectrum.

components in both the converter- and grid-side currents are neglected regardless of the existence of CM components in the converter generated output voltage. Based on this, for the purpose of the LCL filter design in a three-wire system, (10) should be used while only considering the DM components in the converter output voltage. This can be realized by separating the CM components from the original voltage spectrum. In other words, the use of (10) should neglect the terms with n equals to zero and the triple multiples. Besides, for practical use of (10) to calculate the voltage harmonic at a specific harmonic order, some simplifications can be adopted to reduce the calculation time with adequate accuracy. Fig. 4 describes the procedures for the practical calculation of the specified voltage harmonic. Usually the first ten terms in the Fourier series expansion of the periodic waveform can give a satisfactory approximation [16]. The same approximation also holds for the Jacobi-Anger expansion because of the rapid roll-off of the Bessel function magnitudes [20]. Hence, the maximum value for both r and k shown in Fig. 4 is taken as 10.

To validate the correctness of the derived model without losing generality, the voltage spectrum generated by the analytical model is compared with the circuit simulation results under SPWM, THIPWM and SVPWM [20]. Fig. 5 shows the simulated voltage harmonic spectra compared with the analytically constructed spectrum calculated by (10) under sinusoidal and triangle variable frequency profiles in the three different modulation cases. The profiles are implemented with f_{c0} =24.05 kHz and f_{b} =1 kHz. The remaining system parameters can be found in Table I. Since only the first carrier band spectrum is typically concerned with the design of the LCL filter only the first carrier band spectra are shown in Fig. 5. In each modulation case, the CM and DM voltage spectra of either simulation or analytical results are separated and compared respectively. The results illustrate that (10) can predict the harmonic spectra of the VSC generated voltage well, which match the simulated results with relatively good accuracy. The results depicted hence verify the correctness of the model as well as the proposed calculation algorithm.

D. Applicability to Low Switching Frequency

The two assumptions mentioned in Section II-B require a relatively larger centered switching frequency and narrowed variation band of the variable switching frequency to guarantee a reasonable approximation of the coefficient A_{mn} for VSF-PWM as described in (11), where the following substitution is made:

$$n\frac{\omega_{\mathrm{o}}}{\omega_{\mathrm{c}}(t)} \implies n\frac{\omega_{\mathrm{o}}}{\omega_{\mathrm{c0}}} \tag{14}$$

Still, it is necessary to quantify the applicable range of the centered switching frequency for the derived analytical spectrum model. In order to assess the accuracy of the model under different centered switching frequency other than 24.05 kHz, the voltage spectra given by the simulation and analytical results are compared for different cases of f_{c0}, namely $f_{\mathrm{c0}} = 2$ kHz, 4 kHz, 8 kHz, 10 kHz, 12 kHz and 16 kHz respectively. The variation band f_{b} is always selected to be one-tenth the centered switching frequency to exhibit a fair comparison between different cases. Fig. 6 presents the root-mean-square error (RMSE) and the critical harmonic error between the simulated and analytical spectra under various modulation methods and periodic switching frequency profiles. The root-mean-square error ε_{RMSE} is calculated by

$$\varepsilon_{\mathrm{RMSE}} = \sqrt{\frac{\sum_{k=1}^{N}(V_{\mathrm{simu}}(k) - V_{\mathrm{analy}}(k))^2}{N}} \tag{15}$$

where V_{simu} and V_{analy} represent the simulated and analytical voltage spectra and N is the total number of harmonics to be calculated in the spectra. Undoubtedly, the voltage error arises with the lower centered switching frequency applied to the analytical spectrum model. Besides, the error is much greater under 1/4 THIPWM and SVPWM methods compared to SPWM. This is because the voltage harmonics spectra generated by 1/4 THIPWM and SVPWM under CSFPWM with regular sampling is more dependent on the term $n\omega_{\mathrm{o}}/\omega_{\mathrm{c0}}$ compared to the SPWM method [20]. Hence the model becomes less accurate for 1/4 THIPWM and SVPWM under low centered switching frequency since (14) deviates from the assumptions. Lastly, the error in the common-mode voltage components of the spectra is much smaller compared to the differential-mode components. This is because the most common-mode harmonics in the spectra originate from the harmonic from CSFPWM where the side-band n=0. For those

This article has been accepted for publication in a future issue of this journal, but has not been fully edited. Content may change prior to final publication. Citation information: DOI 10.1109/TPEL.2022.3141268, IEEE Transactions on Power Electronics

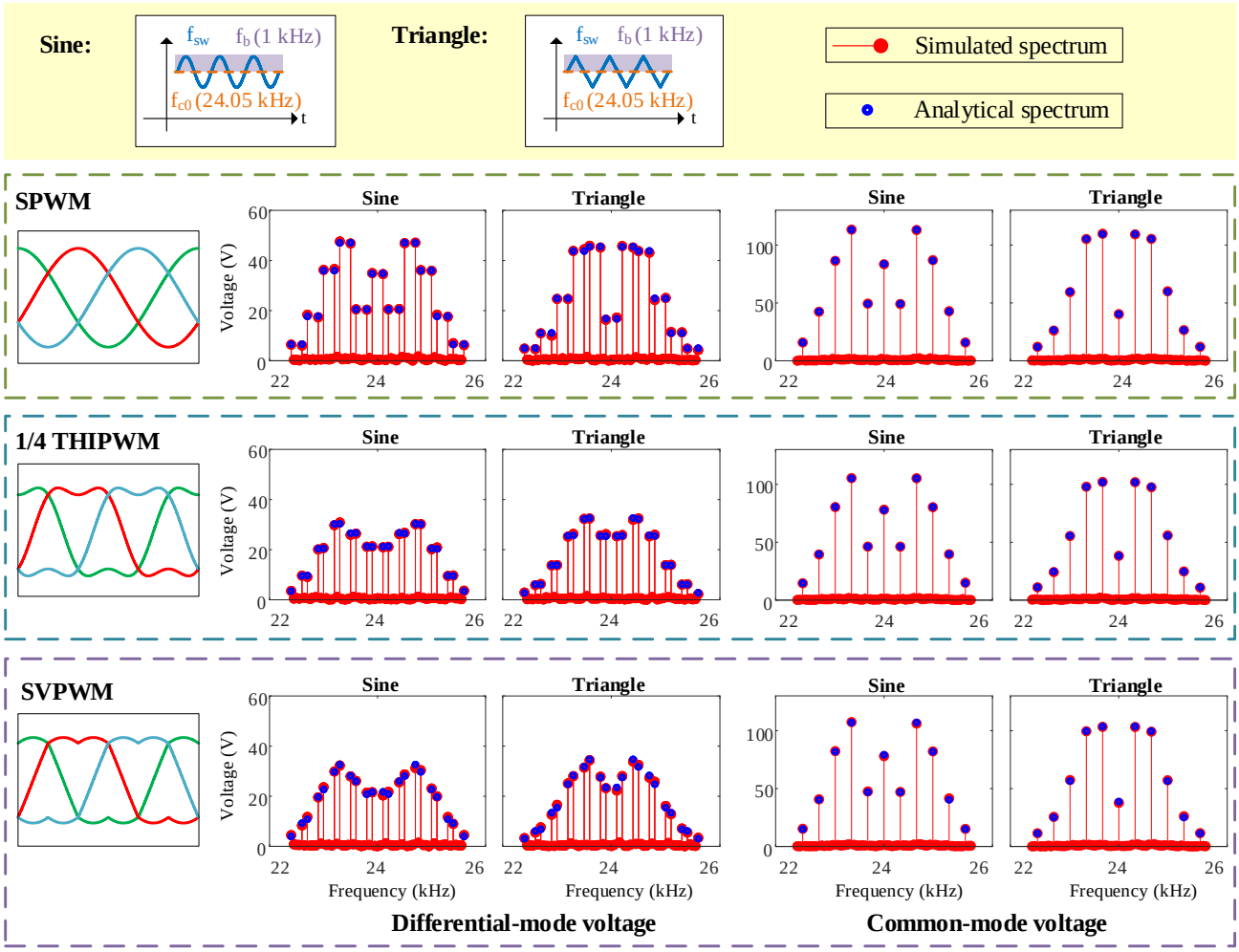

Fig. 5. The simulated and analytical converter output voltage spectrum under different modulations and frequency profiles.

harmonics, the (14) is always valid since the term becomes zero.

In summary, the derived analytical spectrum model becomes less accurate under low centered switching frequency due to the unavoidable symmetrical regular sampling process of the digital implementation of PWM in practice. However, the error is still acceptable if the centered switching frequency f_{c0} is selected to be larger than 4 kHz since the error is less than 4 V, which is relatively small (8%) compared to its critical harmonic magnitude. Usually a design margin of inductance will be considered for the inductor to deal with the inductance variation under high temperature and drop of permeability caused by current bias. Therefore, the proposed model can still be applicable to low centered switching frequency and the recommended range is $f_{c0} \geqslant 4$ kHz.

III. Design Guidelines for Periodic VSFPWM and LCL Filter

Some criteria and guidelines have been developed to assist the LCL filter design for the grid-connected VSC using the constant switching frequency PWM [1], [26]–[28]. The filter parameters are subsequently determined by the constraints defined by the design guidelines. Traditional filter design criteria or guidelines can also be applied with VSFPWM although some changes should be adopted due to the spread-spectrum characteristics. In this section a LCL filter design guideline for VSFPWM is devised aiming to not only satisfy the grid harmonic standards, but also to keep the good performance of current THD and power efficiency close to which would be attained with the utilization of CSFPWM.

A. Design constraints for LCL filter

Neglecting the internal resistance of the inductors and considering no passive damping in the filter, the transfer function from the converter output phase voltage $v_{\mathrm{c}}(s)$ to the grid-side current $i_{\mathrm{g}}(s)$ is expressed as follows:

$$\begin{aligned}\frac{i_{\mathrm{g}}(s)}{v_{\mathrm{c}}(s)} &= \frac{1}{L_{\mathrm{c}}L_{\mathrm{g}}C_{\mathrm{f}}s(s^2+\omega_{\mathrm{res}}^2)} \\ &= \frac{\omega_{\mathrm{res}}^2}{L_{\mathrm{T}}s(s^2+\omega_{\mathrm{res}}^2)}\end{aligned} \tag{16}$$

where L_{c} and L_{g} are the converter-and grid-side inductance of the LCL filter respectively. ω_{res} and L_{T} are the resonance fre-

This article has been accepted for publication in a future issue of this journal, but has not been fully edited. Content may change prior to final publication. Citation information: DOI 10.1109/TPEL.2022.3141268, IEEE Transactions on Power Electronics

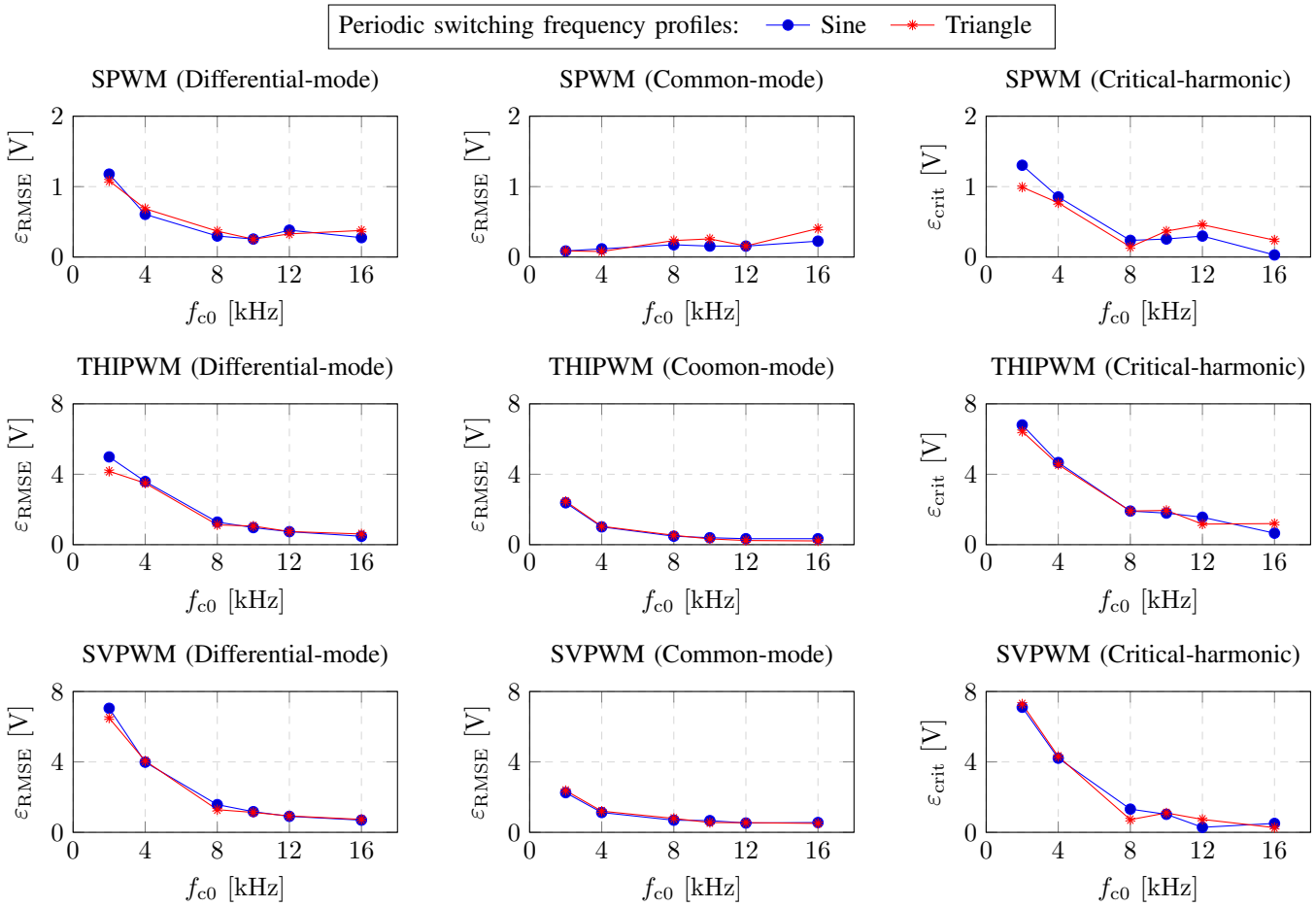

Fig. 6. Errors between the analytical and simulated results under lower centered switching frequency range.

quency and the total inductance of the LCL filter respectively, and expressed as:

$$\omega_{\mathrm{res}} = \sqrt{\frac{L_{\mathrm{c}} + L_{\mathrm{g}}}{L_{\mathrm{c}} L_{\mathrm{g}} C_{\mathrm{f}}}} \tag{17}$$

$$L_{\mathrm{T}} = L_{\mathrm{c}} + L_{\mathrm{g}} \tag{18}$$

Therefore, the attenuation from the voltage to the grid-side current can be represented by the magnitude of the transfer function (16), as follows:

$$Att(\omega) = \left\| \frac{i_{\mathrm{g}}(j\omega)}{v_{\mathrm{c}}(j\omega)} \right\| = \frac{1}{L_{\mathrm{T}}} \cdot \frac{\omega_{\mathrm{res}}^2}{\omega |\omega^2 - \omega_{\mathrm{res}}^2|} \tag{19}$$

Equation (19) shows the attenuation capability of the LCL filter on the voltage harmonics. In grid-tied applications as a general guideline for harmonic compliance the AC filters can be designed to meet the harmonic distortion limits established by the IEEE-519-2014, as depicted in Fig. 1. In medium to high switching frequency operated converters the critical spectra content of the grid-side current should be attenuated to be less than the harmonic limit, namely 0.3% and 0.075% of the fundamental current for odd- and even-order harmonics respectively, noted as I_{IEEE519} in this paper. In constant frequency PWM operation, the output voltage only has few prominent side-band harmonics appearing in the vicinity of the first switching frequency band (m=1). Specifically for SPWM operation, by defining m_{f} as $\omega_{\mathrm{c}}/\omega_{\mathrm{o}}$, the critical frequency is found to be the $(m_{\mathrm{f}} - 2)^{\mathrm{th}}$ order of the fundamental frequency since this voltage harmonic results in the largest current harmonic magnitude after the attenuation of the filter. m_{f} is usually selected to be odd integer so that the critical frequency becomes odd-order harmonic. Thereby, the stricter harmonic limit for the even harmonics can be avoided and the design of the minimum required inductance value is ensured.

The critical current harmonic should be attenuated to be below I_{IEEE519}. In other words, the total inductance L_{T} should be selected to ensure that the critical current harmonic is below the limit set by the standard:

$$Att_{\mathrm{req}} = \frac{I_{\mathrm{IEEE519}}}{V_{\mathrm{crit}}} \tag{20}$$

By using (19) and (20), the minimum required total inductance of the LCL filter for satisfying the standard can be derived as:

$$L_{\mathrm{T-req}} = \frac{\omega_{\mathrm{res}}^2 V_{\mathrm{crit}}}{\omega_{\mathrm{crit}} \left|\omega_{\mathrm{crit}}^2 - \omega_{\mathrm{res}}^2\right| I_{\mathrm{IEEE519}}} \tag{21}$$

From (21), the minimum required total inductance is proportional to the magnitude of the critical voltage harmonic V_{crit} and approximately inverse to the cubic of the critical frequency. Additionally, the minimum total inductance is also

TABLE I
SYSTEM PARAMETERS FOR SIMULATION AND EXPERIMENT

PARAMETER	VALUE
AC side	
Voltage V_{ac} (rms)	230 V
Fundamental frequency f_o	50 Hz
Converter	
Semiconductor	C3M0120090J
Blocking voltage V_B	900 V
Drain current I_D	14 A
Operating power	2.2 kW
V_{dc}	700 V
C_{dc}	365 μF
f_{c0}	24.05 kHz
r_f	0.219
LCL Filter	
Converter-side Inductance L_c	370 μH
Grid-side Inductance L_g	360 μH
Capacitance C_f	5 μF
Modulation	SPWM, SVPWM 1/4 THIPWM

associated with the resonance frequency of the LCL filter. To avoid the instability caused by the filter resonance and to realize a stable grid-side current control, the resonance frequency of the LCL filter should be designed with regard to the so-called critical frequency [29], [30]. The resonance frequency should be larger than one sixth of the switching frequency to attain the inherent stability without extra damping methods applied [31], [32]. In this work, the resonance-switching ratio $r_f = f_{res}/f_{c0}$ is selected to be 0.219 as listed in Table.I and remains fixed during the following designs developed in this paper.

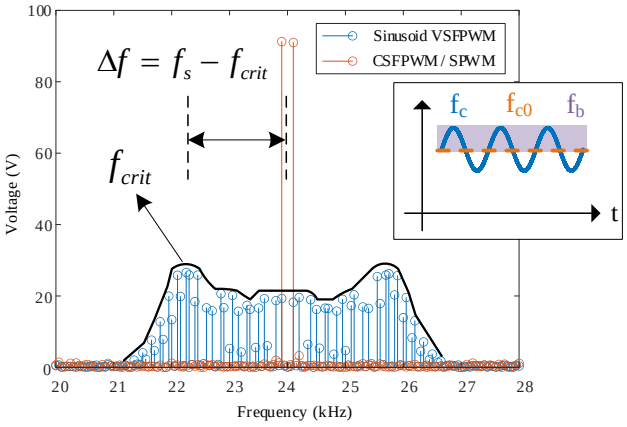

Fig. 7. Critical harmonic frequency and switching frequency variation band for sinusoidal VSFPWM and conventional CSFPWM.

B. Optimized design of f_m, f_b and L_T

When VSFPWM is adopted, the voltage and consequently the current spectra content across the AC filter are spread differently depending on the switching profiles adopted. Therefore the critical harmonic order $(m_f - 2)^{th}$ derived for CSFPWM does not apply to VSFPWM due to the varied spectrum. Moreover, the critical frequency can not be found straightforwardly from the non-intuitive spectrum. However, it is noteworthy that the critical frequency is closely associated with the applied switching profile. Fig. 7 depicts the critical

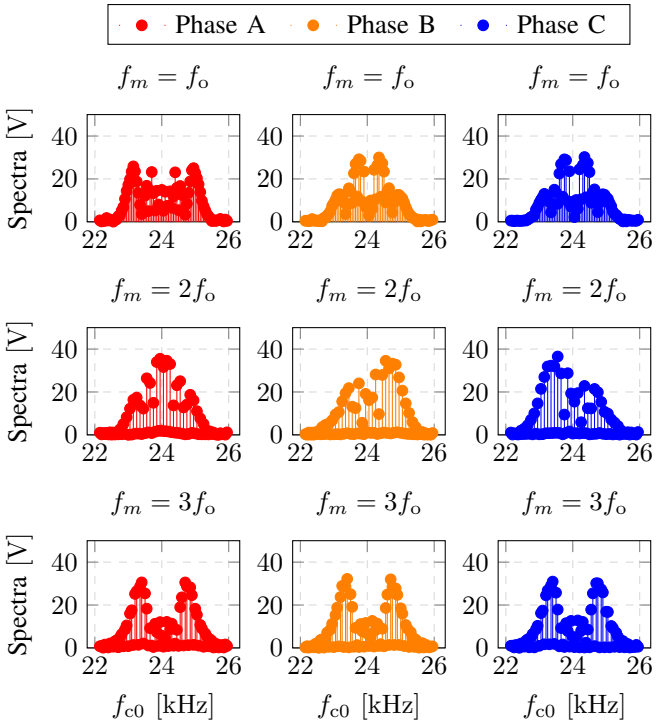

Fig. 8. The differential-mode spectra of the three phase voltages with SVPWM method and triangle periodic switching profile at f_m=f_o, $2f_o$, $3f_o$.

frequency f_{crit} and switching frequency variation band f_b in the spectrum plot by using sinusoidal profile as an example. It is noted that f_{crit} is related to f_b, and hence, the choice of f_b also influences the design of the total inductance L_T of the LCL filter. Besides, V_{crit} is not only associated with f_b but also with the periodic frequency f_m. Therefore, the influence of the design variables f_m and f_b on L_T should be investigated before determining the total inductance value.

Before the derivation of the relation between the critical frequency f_{crit} and f_b, the periodic frequency f_m should be firstly determined. Fig. 8 presents the three phase converter voltage spectra under f_m equal to different multiples of f_o. Except the case of f_{c0} = $3f_o$, the voltage spectra between three phases are not identical in magnitude for rest cases. Theoretically, when a single triangle carrier wave is used for the modulation of all three phases, f_m should be chosen as triple multiples of the fundamental frequency f_o to ensure that the harmonic spectra of the VSC output voltages remain symmetrical between three phases. That is:

$$f_m = 3kf_o \tag{22}$$

where k is a non-zero positive integer value. Similar to the CSFPWM case, the side-band harmonics including the critical

harmonic are expected to be placed at an odd harmonic order. If m_{f} is defined as $f_{\mathrm{c0}}/f_{\mathrm{o}}$ for the VSFPWM operation, then the requirement can be expressed as:

$$\begin{cases} nf_{\mathrm{o}} + lf_{\mathrm{m}} = (2N-1)f_{\mathrm{o}} & m_{\mathrm{f}} \text{ is even} \\ nf_{\mathrm{o}} + lf_{\mathrm{m}} = 2Nf_{\mathrm{o}} & m_{\mathrm{f}} \text{ is odd} \end{cases} \tag{23}$$

where N is the arbitrary integer value. By using (22), (23) can be simplified as:

$$\begin{cases} n + 3l \cdot k = 2N-1 & m_{\mathrm{f}} \text{ is even} \\ n + 3l \cdot k = 2N & m_{\mathrm{f}} \text{ is odd} \end{cases} \tag{24}$$

By analyzing the voltage spectrum with CSFPWM, it has been found that only even side-band harmonics appear in the spectrum, which means that n is an even number. Therefore, the first argument where m_{f} is eliminated because there exists no such an integer k satisfying the first condition for any values of n and l. The second condition holds if k is selected to be an even number. Hence, the periodic frequency f_{m} of the switching frequency should satisfy:

$$f_m = 6kf_o \tag{25}$$

The critical frequency f_{crit} is obtained by finding the most dominant harmonic by applying a normalized attenuation of the LCL filter to the spectrum of the output voltage. The expression of the normalized attenuation is given by:

$$Att_{\mathrm{norm,LCL}}(\omega) = \frac{\omega_{\mathrm{res}}^2}{\omega|\omega^2 - \omega_{\mathrm{res}}^2|} \tag{26}$$

Hence, the normalized critical harmonic current $I_{\mathrm{crit,norm}}$ can be found by:

$$I_{\mathrm{crit,norm}} = max\big(\big|V_{\mathrm{c}}(\omega)\big| \cdot Att_{\mathrm{norm,LCL}}(\omega)\big) \tag{27}$$

The critical voltage harmonic is expressed as:

$$V_{\mathrm{c}}(\omega) = \sum C_{\mathrm{mnl}} \tag{28}$$

where ω satisfies

$$\omega = 2\pi(mf_{\mathrm{c0}} + nf_{\mathrm{o}} + lf_{\mathrm{m}}) \tag{29}$$

In (29), the multiple of the carrier harmonic m is selected to be 1 since the critical harmonic exists in the side bands of the first carrier harmonic. The critical voltage harmonic then is calculated according to the algorithm described in Fig. 4. Finally, the critical frequency f_{crit} hence can be found by retrieving the corresponding frequency from $I_{\mathrm{crit,norm}}$. As a result, the distance Δf between the critical frequency f_{crit} and the centred switching frequency f_{c0} is obtained. The required total inductance $L_{\mathrm{T-req}}$ can be subsequently derived by using (21).

In order to find the optimal f_{b} and the consequent minimal $L_{\mathrm{T-req}}$, the algorithm shown in Fig. 9 has been proposed. For the certain modulation method and VSFPWM profile shape, the algorithm requires the converter specifications such as the rated grid voltage and current V_{g} and I_{g}, the modulation index M and the fundamental frequency f_o. Besides, f_{c0} and f_{m} of the VSFPWM, the current harmonic limit, and the filter resonance frequency are also input to the algorithm. The algorithm finds the critical frequency and the associated

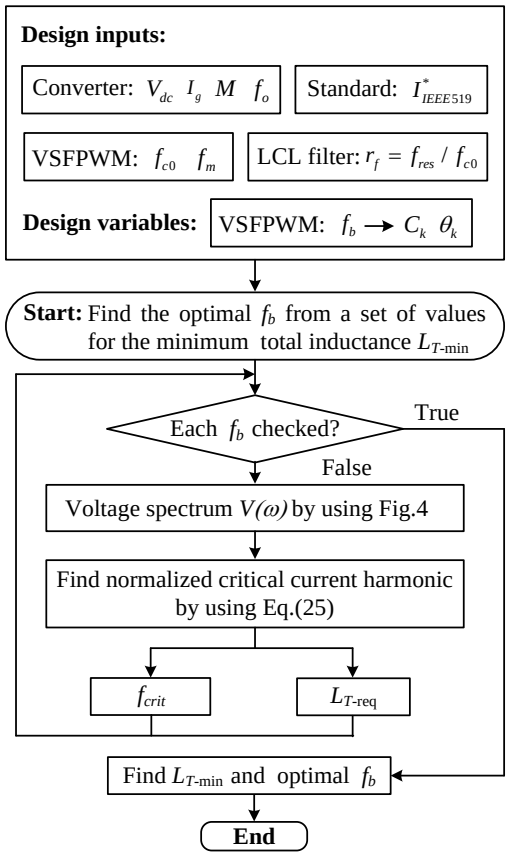

Fig. 9. Algorithm for optimal f_b to achieve minimum total inductance L_T.

TABLE II
THE DESIGNED OPTIMAL SWITCHING PROFILES

VSFPWM switching Profile	f_{b} (Hz)	$L_{\mathrm{T-req}}$ (μH)
SPWM		
CSFPWM	——	2560
VSFPWM sinusoid profile	2400	1115
VSFPWM triangle profile	3900	947
1/4 THIPWM		
CSFPWM	——	1330
VSFPWM sinusoid profile	1900	772
VSFPWM triangle profile	3700	667
SVPWM		
CSFPWM	——	1565
VSFPWM sinusoid profile	2200	810
VSFPWM triangle profile	3700	710

required total inductance $L_{\mathrm{T-req}}$ for each f_b from a wide range set of values. Finally, the minimum $L_{\mathrm{T-req}}$ can be found by traversing the whole range and the related f_{b}.

With the algorithm shown in Fig. 9, the relations between f_{b} and Δf are presented in Fig. 10. From Fig. 10, Δf shows a different staircase quasi-linear relation with f_{b} under the SPWM, 1/4 THIPWM and SVPWM methods. Besides, the minimum required total inductance under various f_b is also found by using the algorithm and presented in Fig. 11. Regardless of the modulation method, the required total inductance under the periodic switching profiles always drops with the

This article has been accepted for publication in a future issue of this journal, but has not been fully edited. Content may change prior to final publication. Citation information: DOI 10.1109/TPEL.2022.3141268, IEEE Transactions on Power Electronics

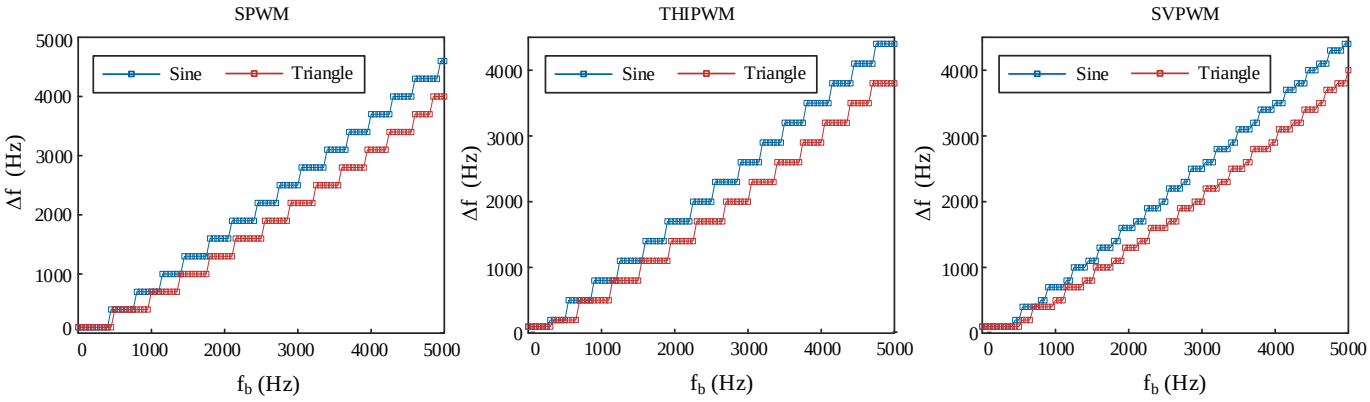

Fig. 10. The relation between f_b and Δf under various VSFPWM methods and frequency profiles.

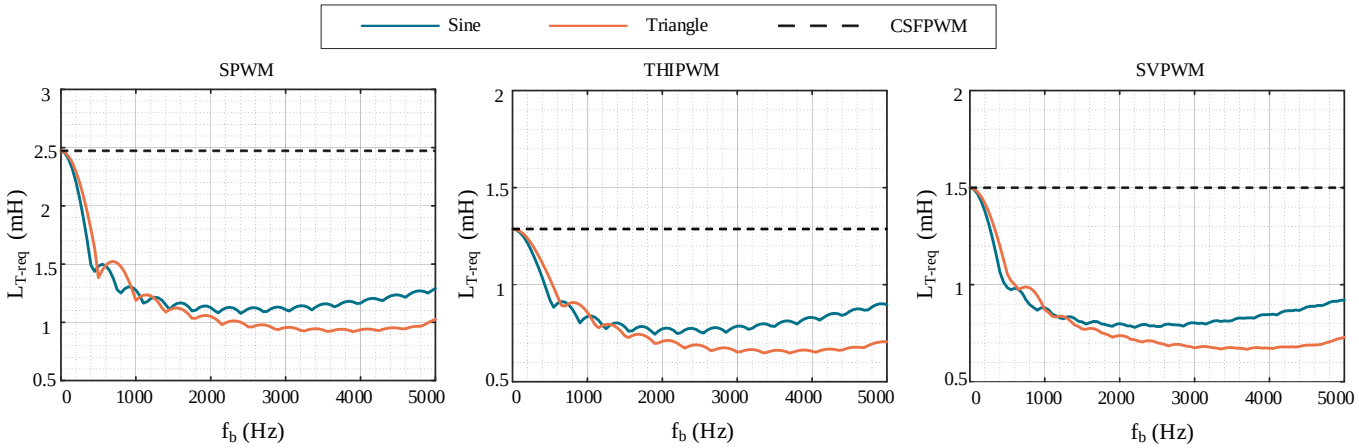

Fig. 11. The relation between the require total inductance L_T and f_b under various VSFPWM methods and frequency profiles.

initial increase of f_{b} and then begins to increase from a certain value of f_{b}. The optimal points giving the maximum inductance drop are summarized in Table.II. Compared with the CSFPWM, the sinusoid and triangle VSFPWM profiles lead to a remarkable reduction of the required total inductance. Specifically, the triangle profile can result in a larger reduction compared with the sinusoid profile, which is around 50%–60% depending on the modulation method. Compared with SPWM, both SVPWM and 1/4 THIPWM methods require less total inductance $L_{\mathrm{T-req}}$, but also they feature similar inductance drop tendency.

C. Selection of L_c, L_g and C_f

As a constraint for the filter design, the maximum AC filter capacitance C_{f} is limited by the maximum allowable reactive power to be compensated by the VSC which is consumed by this component at the PCC (point-of-coupling). This is important to limit the circulating reactive power which could reduce the converter power efficiency, particularly at partial or low load conditions. Hence, the filter capacitance should fulfil the requirement:

$$C_{\mathrm{f}} < q \cdot \frac{S_{\mathrm{N}}}{3\omega_{\mathrm{o}} V_{\mathrm{ac}}^2} \tag{30}$$

where S_{N} is the rated power of the system and q is ratio of the device fundamental reactive power and set to 5% in this paper.

As aforementioned, r_{f}, namely the ratio between the resonance and switching frequency, is set to be larger than 1/6 to achieve the stability of grid-side current control with the inherent damping under the continuous PWM methods adopted in this paper [31], [32]. Hence, the extra active damping means can be avoided, which simplifies the potential controller. The converter- and grid-side inductance will be determined subsequently after the value of the total inductance L_T is selected based on (21). By combining (17) and (18), L_c and L_g are derived by:

$$L_{\mathrm{c,g}} = \frac{L_{\mathrm{T}}}{2} \pm \sqrt{\frac{L_{\mathrm{T}}^2}{4} - \frac{L_{\mathrm{T}}}{\omega_{\mathrm{res}}^2 C_{\mathrm{f}}}} \tag{31}$$

where the total inductance satisfies

$$L_{\mathrm{T}} \geqslant \frac{4}{\omega_{\mathrm{res}}^2 C_{\mathrm{f}}} \tag{32}$$

Besides, the upper limit of the total inductance is constrained by the maximum converter phase voltage and the rated grid-side current by considering the voltage drop of L_{T} [1].

$$L_{\mathrm{T}} \leqslant \frac{\sqrt{\frac{V_{\mathrm{dc}}^2}{6} - V_{\mathrm{ac}}^2}}{\omega_{\mathrm{o}} I_{\mathrm{g}}} \tag{33}$$

Usually the larger value in (31) is selected for L_c for the purpose of limiting the converter current ripple. The LCL filter parameters designed for the SVPWM operation with triangle VSFPWM profile are listed in Table I.

D. Influence on the Switching Loss and Control

The semiconductor switching loss can be modeled as [33]:

$$P_{\rm sw} = \frac{f_{\rm c} V_{\rm dc}}{2\pi V_{\rm ref}} \int_0^{2\pi} E_{\rm on,off,rr} {\rm d}\omega_{\rm o} t \tag{34}$$

where $V_{\rm ref}$ is the normalized DC voltage provided in datasheet. $E_{\rm on,off,rr}$ represents the switching energies and can be expressed as second-order polynomial function of the current:

$$E_{\rm on,off,rr} = ai(t)^2 + bi(t) + c \tag{35}$$

$$i(t) = I\sin(\omega_{\rm o} t + \varphi) \tag{36}$$

Combine (6), (25) (34), (35) and (36), the switching loss model for the periodic VSFPWM becomes:

$$\begin{aligned} P_{\rm sw} =& P_{\rm sw0} + \frac{V_{\rm dc}}{2\pi V_{\rm ref}} \sum_{k=1}^{\infty} \Big(\int_0^{2\pi} \Big(-\frac{aI^2\cos(2\omega_{\rm o} t + 2\varphi)}{2} + \\ & bI\sin(\omega_{\rm o} t + \varphi) \Big) + c + \frac{aI^2}{2} \Big) \cdot C_{\rm k} \sin(6k\omega_{\rm o} t + \theta_{\rm k}) {\rm d}\omega_{\rm o} t \Big) \\ =& P_{\rm sw0} \end{aligned} \tag{37}$$

where $P_{\rm sw0}$ is the switching loss under CSFPWM with the centered switching frequency $f_{\rm c0}$ and is expressed as:

$$P_{\rm sw0} = \frac{f_{\rm c0} V_{\rm dc}}{2\pi V_{\rm ref}} \int_0^{2\pi} E_{\rm on,off,rr} {\rm d}\omega_{\rm o} t \tag{38}$$

The second term in (37) becomes zero due to the orthognality between the integrated functions regardless the current phase angle φ. This implies this conclusion applies to all three phases of the PWM converter. Besides, (37) means that the proposed periodic PWM method does not cause extra semiconductor switching loss compared to CSFPWM and hence will not bring additional thermal stress on the semiconductor devices.

Since the current harmonics are concerned in this paper, the current controller for the PWM converter should be designed to be capable of rejecting the low-order harmonics below the Nyquist frequency ($f_{\rm c}/2$) of the system. Therefore, minimum applicable centered switching frequency can be identified by setting the minimum possible Nyquist frequency to be greater than the mostly concerned low-order harmonic frequencies. In IEEE519 standard, for instance, the harmonics only count up to 35th order. Hence, we have:

$$\frac{f_{\rm c-min}}{2} = \frac{f_{\rm c} - f_{\rm b}}{2} > 35 \cdot f_{\rm o} \tag{39}$$

Based on [17], [18], $f_{\rm b}$ should satisfy:

$$f_{\rm b} \leqslant \frac{f_{\rm c0} - 2f_{\rm m}}{3} \tag{40}$$

to avoid the overlapping of the spectra of the first and second carrier frequency regions. Substitute (25) into (29) and the minimum centered switching frequency can be found by:

$$f_{\rm c0} > 99 f_{\rm o} \tag{41}$$

Therefore, $f_{\rm c0}$ is greater than 5 kHz for our typical application. Combine the range $f_{\rm c0} \geqslant$4 kHz derived in Section. II-D, $f_{\rm c0}$ is be greater than 5 kHz for the considerations of both the low-order harmonics rejection capability for the potential current controller and applicability of the derived analytical spectrum model.

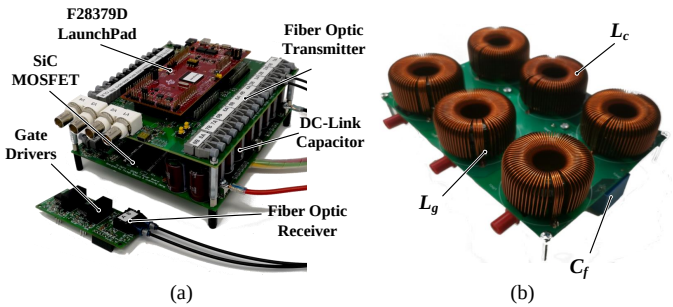

Fig. 12. Experimental setup: (a) VSC; and (b) LCL filter.

IV. Simulation and Experimental Results

To validate the correctness of the spectrum models and the optimal switching profiles, both simulation and experimental tests are conducted and compared with various PWM methods on the studied three-phase three-wire two-level VSC depicted in Fig. 2. Firstly, a MATLAB/SIMULINK based simulation is carried out. Thereafter, the adopted periodic switching profiles

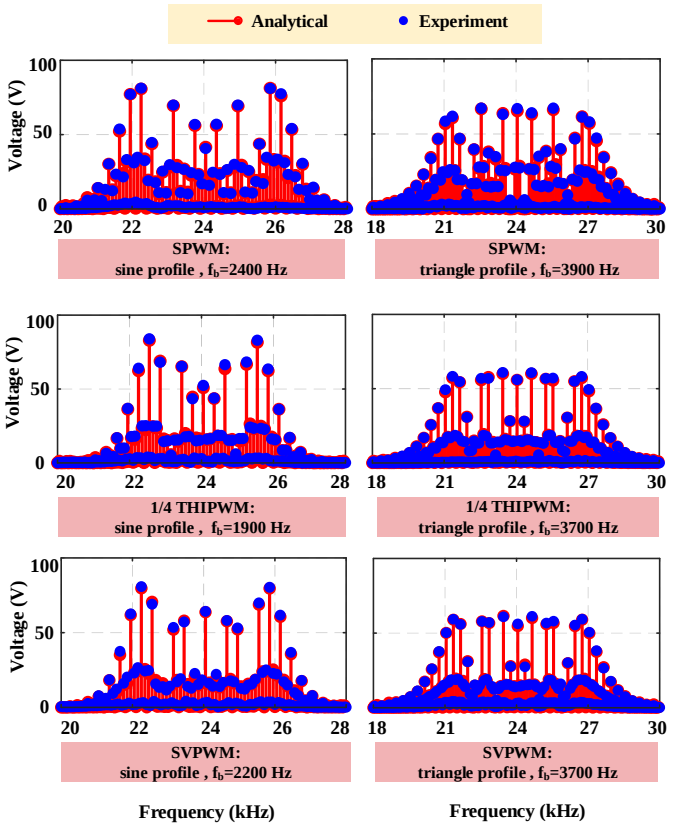

Fig. 13. Comparison between the analytical and experimental results of the converter output voltage spectra of the 1st carrier band under various switching profiles and PWM methods.

This article has been accepted for publication in a future issue of this journal, but has not been fully edited. Content may change prior to final publication. Citation information: DOI 10.1109/TPEL.2022.3141268, IEEE Transactions on Power Electronics

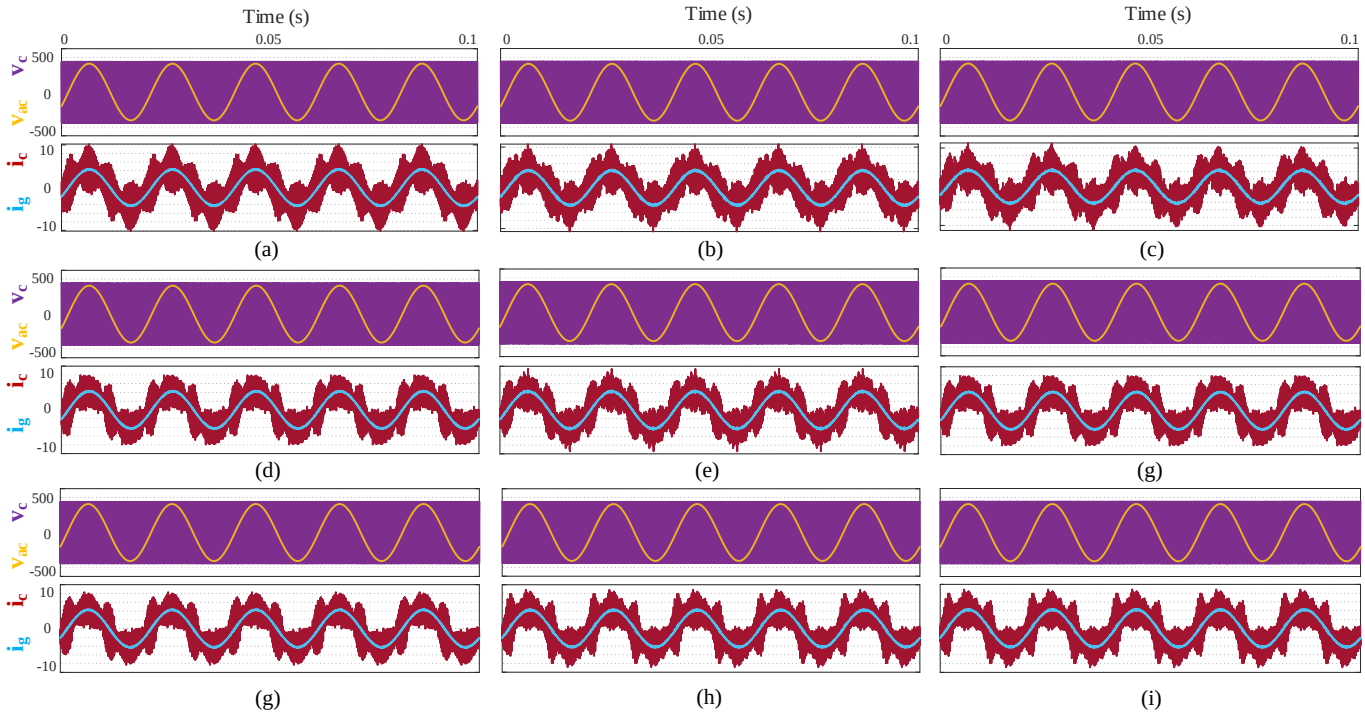

Fig. 14. Simulation results of the three-phase three-wire two-level converter under various switching profiles and PWM methods: (a) SPWM—constant switching frequency (b) SPWM—sinusoid profile: f_b=2400 Hz (c) SPWM—triangle profile: f_b=3900 Hz (d) THIPWM—constant switching frequency (e) THIPWM—sinusoid profile: f_b=1900 Hz (f) THIPWM—triangle profile: f_b=3700 Hz (g) SVPWM—constant switching frequency (h) SVPWM—sinusoid profile: f_b=2200 Hz (i) THIPWM—triangle profile: f_b=3700 Hz. Note that only one of the three phase waveforms are recorded.

are realized on a digital-controlled hardware platform with the DSP TMS320F28379D from Texas Instruments. The key specifications of the considered VSC are listed in Table I.

In order to further validate the correctness and feasibility of the proposed model, the switching profiles listed in Table II are experimentally realized in a 5 kW prototype based on the power electronic circuit shown in Fig. 2. This is shown in Fig. 12. Therein, for the power semiconductors three hard-paralled SMD packaged 900 V Silicon Carbide (SiC) MOSFETs are used per necessary active switch. For the rated power only natural convection PCB mounted heat sinks are necessary for the thermal management of the devices junction temperatures. A 200 MHz dual core Micro Controller Unit (MCU) from Texas Instruments assembled in a LaunchPad development kit is used. A master PC is used to control the operating modes programmed in the MCU through a USB communication link which is electrically isolated by a XDS100v2 debug probe. Additionally, to achieve a high Common-Mode Rejection Ratio (CMRR) and also for human safety reasons the control and the power boards are interconnected through optical fiber links. For the implementation of the conventional d-q controller all the necessary Analog-to-Digital Conversions (ADC) of the inverter required measurements, namely the AC converter-and grid-side terminal currents, and the AC grid voltages and DC terminal voltages, are performed in the power board using 10 MHz delta-sigma modulators. The measured data is transmitted to the available sigma-delta filter channels of the MCU through a 50BMd fiber optic transmitter. The LCL filter board depicted in Fig. 12(b) is built with two toroidal-core inductors with 370 μH and 360 μH respectively, which are measured with an impedance analyser. A film capacitor of 5 μF is used as the AC filter capacitor. The component value selection was devised using the design guideline presented in Section III while considering the VSFPWM strategy employing 1/4 THIPWM and triangular frequency profile. As it will be shown in the following this strategy leads to the smallest requirement of L_T for the operational condition listed in Table I. In experiments, the three-phase two-level converter is operated in the inverter mode operating at full power factor at PCC. All of the experimental waveforms and data used in this paper are recorded by the oscilloscope YOKOGAYA DLM2054, and the current THD and power conversion efficiency of the converter are tested by the power analyzer YOKOGAYA WT500.

A. *Validation of Periodic VSFPWM Spectrum Model*

The correctness of the analytical VSFPWM spectrum model has already been verified by comparing the simulated and analytical converter output voltage spectra, which is shown in Fig. 5. The nine different switching profiles listed in Table II are examined by both simulation and experiment. The simulation and experimental results with the measured waveform are shown in Fig. 14 and Fig. 15 respectively. Due to the limitation of the oscilloscope channels, only one phase output current/voltage waveforms are recorded in the experiment. By using the fast Fourier-transform method on the converter generated output voltage (or v_c), i.e., the purple waveform in Fig. 15, the generated output voltage's spectra from the experimental results are obtained and presented in

This article has been accepted for publication in a future issue of this journal, but has not been fully edited. Content may change prior to final publication. Citation information: DOI 10.1109/TPEL.2022.3141268, IEEE Transactions on Power Electronics

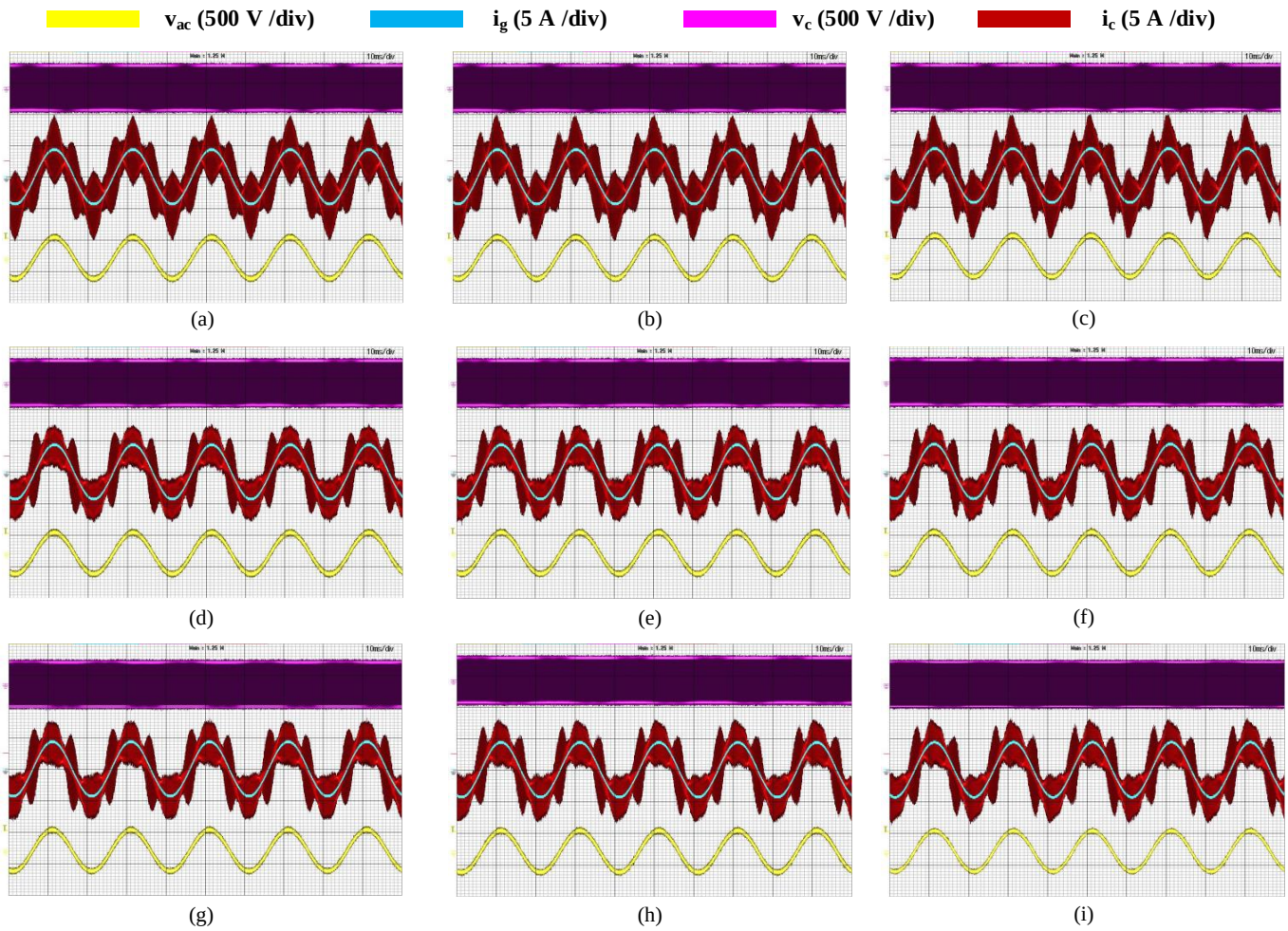

Fig. 15. Experimental results of the three-phase three-wire two-level converter under various switching profiles and PWM methods: (a) SPWM—constant switching frequency (b) SPWM—sinusoid profile: f_{b}=2400 Hz (c) SPWM—triangle profile: f_{b}=3900 Hz (d) THIPWM—constant switching frequency (e) THIPWM—sinusoid profile: f_{b}=1900 Hz (f) THIPWM—triangle profile: f_{b}=3700 Hz (g) SVPWM—constant switching frequency (h) SVPWM—sinusoid profile: f_{b}=2200 Hz (i) THIPWM—triangle profile: f_{b}=3700 Hz. Note that only one phase waveforms are recorded.

Fig. 13, in comparison with the spectra constructed by the proposed spectrum model described in Section II.

It can be noted that the spectra from the experimental results match the analytical ones well in all PWM methods and periodic switching profiles. With the analysis on the spectra, the maximum discrepancy between the two spectra is 1.7 V, which is 0.5% of the fundamental voltage and hence can be regarded to be negligible from the design point of view. From the spectra shown in Fig. 13, it can be noted that the triangle profiles in fact exhibits a more evenly spread spectrum compared to the sinusoid profile. This finally results in a smaller critical voltage harmonic requirement to be filtered out. The difference of the magnitude between the critical voltage in the spectra is reflected by the difference of the required inductance shown in Fig. 11. By analysing the critical voltages of the six shown spectra, it is found that the 1/4 THIPWM with the triangle profile (f_{b}) results in the smallest magnitude of the critical voltage, which implies that the minimum value of the required inductance is obtained for this operating case. Besides, the magnitude of the critical voltages are found to be positively correlated to the required inductance values shown in Table.II. Thereafter, it can be concluded that the analytical model of the periodic VSFPWM spectrum is verified to be correct based on the analysis from the simulation and experimental results.

B. Validation of the optimal switching profile

Beside the validation of the VSFPWM spectrum model, the design of the optimal switching profile is also validated by the simulation and experimental tests. The parameters in Table I are used for both the simulations and experiments. Fig. 14 shows the simulation results of the converter output voltage v_{c}, converter-side current i_{c}, grid-side current i_{g} and the AC voltage v_{ac} under the nine designed switching profiles listed in Table II. The AC voltage v_{ac} has a peak value of 325 V while the grid-side current has a peak value of 4.3 A. It can be seen that the periodic switching profiles works well under various PWM methods. The current ripples in the converter-side inductors are significantly attenuated by the adopted LCL filter and the grid-side current i_{g} exhibits a good sinusoidal waveform with low THD. Fig. 15 presents the experimental results of the three-phase two-level inverter under the designed

This article has been accepted for publication in a future issue of this journal, but has not been fully edited. Content may change prior to final publication. Citation information: DOI 10.1109/TPEL.2022.3141268, IEEE Transactions on Power Electronics

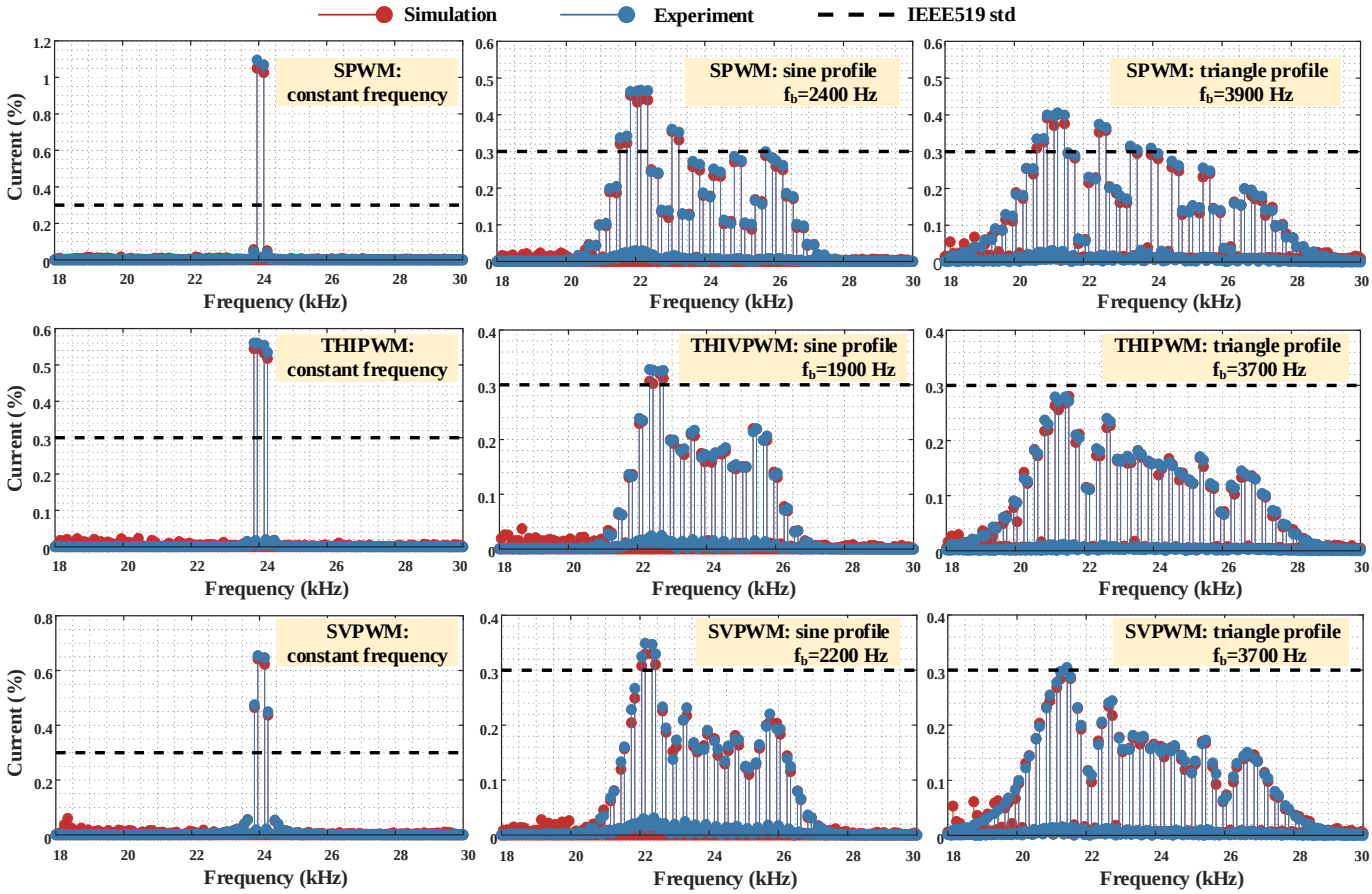

Fig. 16. The grid-side current harmonic spectrum of the 1st carrier frequency side-bands, derived from the experimental and simulation results.

switching profiles. The experimental converter output phase voltage $v_{\rm c}$, the converter-side current $i_{\rm c}$, the grid-side current $i_{\rm g}$ and the AC voltage $v_{\rm ac}$ match well the simulation results in terms of waveforms and values. From the results, it can be seen that the switching harmonics in the currents are significantly attenuated by the adopted LCL filter. However, in order to validate the effectiveness of the implemented filter and switching profiles, the grid-side current spectra are required for further analysis. By extracting the data of the grid-side currents from both the simulation and experiment results, their corresponding spectra are obtained and subsequently depicted in Fig. 16 in comparison to the limits defined by the current harmonic standard.

First, it can be clearly seen that the two current spectra obtained from the simulation and experiment results match each other with a good accuracy under the various PWM methods and switching profiles. The results of the normalized critical current harmonic are summarized in Table III for the intuitive comparison. By comparing the results for different switching profiles with certain modulation method, it is found that the critical current harmonic drops significantly with VSF-PWM profiles compared with CSFPWM. Specifically, triangle profile results in the largest reduction (more than 50%) of the critical current harmonic. Besides, a negligible increment of the THD (Total Harmonic Distortion) is observed in the grid-side current when the VSFPWM profiles are implemented

TABLE III
THE FILTERING INDUCTANCE REQUIRED BY THE IEEE519 STANDARD

Switching Profile	$I_{\rm crit}$ (%)		THD (%)	Efficiency (%)
	Simulation	Experiment	Experimental	Measurement
SPWM				
CSFPWM	1.05	1.07	1.14	98.00
Sinusoid: f_b=2400 Hz	0.453	0.463	1.19	97.86
Triangle: f_b=3900 Hz	0.402	0.408	1.19	97.80
1/4 THIPWM				
CSFPWM	0.545	0.560	1.00	98.00
Sinusoid: f_b=1900 Hz	0.320	0.325	1.07	98.03
Triangle: f_b=3700 Hz	0.267	0.280	1.06	97.94
SVPWM				
CSFPWM	0.642	0.654	1.00	98.05
Sinusoid: f_b=2200 Hz	0.33	0.345	1.04	98.02
Triangle: f_b=3700 Hz	0.292	0.298	1.04	98.07

compared to the relevant CSFPWM. Meanwhile, as shown in Table III, the system efficiency also remains nearly unchanged with the implemented VSFPWM profiles.

Additionally, it can be noted that the 1/4 THIPWM method has the overall best current harmonic performance compared with SPWM and SVPWM, when the same filter and switching profile are used. More specifically, the 1/4 THIPWM with the triangle profile ($f_{\rm b}$) shows the minimum critical current

harmonic compared with the rest switching profiles under the same LCL filter. In other words, 1/4 THIPWM demands the minimum inductance for the LCL filter to achieve the same current harmonic performance. Therefore, the 1/4 THIPWM with triangle switching profile is regarded as the optimal design choice for the implemented system. Besides, it can be seen that the experimental critical current harmonic values are slightly larger than the simulation ones for all the switching profiles. This implies that the total inductance of the LCL filter used in experiment is slightly smaller than 730 μH. This small difference is acceptable considering the possible variation of core permeability with the current bias during the practical implementation of the LCL filter. Therefore, it can be concluded that the VSFPWM following the suggested LCL filter design guideline developed in Section III does not substantially influence the THD and efficiency of the system while remarkably lowering the critical harmonic of the grid-side current.

V. Conclusion

This work has proposed a generic voltage spectrum model for the periodic variable switching frequency modulations in a three-phase three-wire two-level VSC. A practical algorithm has also been proposed to make the spectrum calculation feasible. Besides, this work also presents a novel algorithm to find the optimal periodic profiles, which leads to the minimum required inductance for the LCL filter while meeting the IEEE519 current harmonic standard. Based on such an algorithm, a LCL filter design guideline was devised. Herein, typical periodic variable frequency waveform profiles such as triangle and sinusoid were studied and implemented. The correctness and feasibility of the proposed periodic VSFPWM spectrum model and their implementation were verified by both simulation and experimental results. The results show that the current THD of the grid-side connection and system efficiency will not be influenced by the VSFPWM under the same AC filter while the critical harmonic is reduced substantially. The optimal periodic switching profiles can lead to a 50% reduction of the required filter inductance compared to the CSFPWM under various PWM methods, implying a significantly reduced filter size and increased power density. Besides, for the specified converter system the 1/4 THIPWM with a specific triangle switching profile requires the minimal inductance compared with the other studied profiles.

References

[1] K. Jalili and S. Bernet, "Design of *lcl* filters of active-front-end two-level voltage-source converters," *IEEE Transactions on Industrial Electronics*, vol. 56, no. 5, pp. 1674–1689, 2009.

[2] S. Hoffmann, E. Hoene, O. Zeiter, K.-D. Lang, and G. Feix, "Reducing inductor size in high frequency grid feeding inverters," in *Proceedings of PCIM Europe 2015; International Exhibition and Conference for Power Electronics, Intelligent Motion, Renewable Energy and Energy Management*, pp. 1–8, 2015.

[3] B. Zaidi, A. Videt, and N. Idir, "Optimization method of cm inductor volume taking into account the magnetic core saturation issues," *IEEE Transactions on Power Electronics*, vol. 34, no. 5, pp. 4279–4291, 2019.

[4] K. Park, P. Klaus, and R. M. Burkart, "Spread spectrum modulation for lcl filter design," in *2019 20th International Symposium on Power Electronics (Ee)*, pp. 1–6, 2019.

[5] Z. Quan, Y. W. Li, and C. Jiang, "Design of interleaved converters with minimum filtering requirement," in *2019 IEEE Applied Power Electronics Conference and Exposition (APEC)*, pp. 404–411, 2019.

[6] M. Schweizer, T. Friedli, and J. W. Kolar, "Comparative evaluation of advanced three-phase three-level inverter/converter topologies against two-level systems," *IEEE Transactions on Industrial Electronics*, vol. 60, no. 12, pp. 5515–5527, 2013.

[7] M. Malinowski, K. Gopakumar, J. Rodriguez, and M. Perez, "A survey on cascaded multilevel inverters," *IEEE Trans. Ind. Electron.*, vol. 57, pp. 2197 – 2206, 08 2010.

[8] J. Xu, J. Han, Y. Wang, S. Habib, and H. Tang, "A novel scalar pwm method to reduce leakage current in three-phase two-level transformer-less grid-connected vsis," *IEEE Transactions on Industrial Electronics*, vol. 67, no. 5, pp. 3788–3797, 2020.

[9] J. Xu, J. Han, Y. Wang, M. Ali, and H. Tang, "High-frequency sic three-phase vsis with common-mode voltage reduction and improved performance using novel tri-state pwm method," *IEEE Transactions on Power Electronics*, vol. 34, no. 2, pp. 1809–1822, 2019.

[10] S. Kaboli, J. Mahdavi, and A. Agah, "Application of random pwm technique for reducing the conducted electromagnetic emissions in active filters," *IEEE Transactions on Industrial Electronics*, vol. 54, no. 4, pp. 2333–2343, 2007.

[11] A. C. B. Kumar and G. Narayanan, "Variable-switching frequency pwm technique for induction motor drive to spread acoustic noise spectrum with reduced current ripple," *IEEE Transactions on Industry Applications*, vol. 52, no. 5, pp. 3927–3938, 2016.

[12] D. Jiang and F. Wang, "A general current ripple prediction method for the multiphase voltage source converter," *IEEE Transactions on Power Electronics*, vol. 29, no. 6, pp. 2643–2648, 2014.

[13] X. Mao, R. Ayyanar, and H. K. Krishnamurthy, "Optimal variable switching frequency scheme for reducing switching loss in single-phase inverters based on time-domain ripple analysis," *IEEE Transactions on Power Electronics*, vol. 24, no. 4, pp. 991–1001, 2009.

[14] D. Jiang and F. Wang, "Variable switching frequency pwm for three-phase converters based on current ripple prediction," *IEEE Transactions on Power Electronics*, vol. 28, no. 11, pp. 4951–4961, 2013.

[15] O. Oñederra, I. Kortabarria, I. M. de Alegría, J. Andreu, and J. I. Gárate, "Three-phase vsi optimal switching loss reduction using variable switching frequency," *IEEE Transactions on Power Electronics*, vol. 32, no. 8, pp. 6570–6576, 2017.

[16] Q. Li, J. Chen, and D. Jiang, "Periodic variation in the effect of switching frequency on the harmonics of power electronic converters," *Chinese Journal of Electrical Engineering*, vol. 6, no. 3, pp. 35–45, 2020.

[17] D. Gonzalez, J. Balcells, A. Santolaria, J.-C. Le Bunetel, J. Gago, D. Magnon, and S. Brehaut, "Conducted emi reduction in power converters by means of periodic switching frequency modulation," *IEEE Transactions on Power Electronics*, vol. 22, no. 6, pp. 2271–2281, 2007.

[18] J. Balcells, A. Santolaria, A. Orlandi, D. Gonzalez, and J. Gago, "Emi reduction in switched power converters using frequency modulation techniques," *IEEE Transactions on Electromagnetic Compatibility*, vol. 47, no. 3, pp. 569–576, 2005.

[19] K. Tse, H. S.-H. Chung, S. Ron Hui, and H. So, "A comparative study of carrier-frequency modulation techniques for conducted emi suppression in pwm converters," *IEEE Transactions on Industrial Electronics*, vol. 49, no. 3, pp. 618–627, 2002.

[20] G. Holmes, T. Lipo, and T. Lipo, *Pulse Width Modulation for Power Converters: Principles and Practice*, 01 2003.

[21] J. Chen, D. Sha, J. Zhang, and X. Liao, "An sic mosfet based three-phase zvs inverter employing variable switching frequency space vector pwm control," *IEEE Transactions on Power Electronics*, vol. 34, no. 7, pp. 6320–6331, 2019.

[22] J. Chen, D. Sha, J. Zhang, and X. Liao, "A variable switching frequency space vector modulation technique for zero-voltage switching in two parallel interleaved three-phase inverters," *IEEE Transactions on Power Electronics*, vol. 34, no. 7, pp. 6388–6398, 2019.

[23] H. A. Attia, T. K. S. Freddy, H. S. Che, W. P. Hew, and A. H. El Khateb, "Confined band variable switching frequency pulse width modulation (cb-vsf pwm) for a single-phase inverter with an lcl filter," *IEEE Transactions on Power Electronics*, vol. 32, no. 11, pp. 8593–8605, 2017.

[24] D. Holmes, "The significance of zero space vector placement for carrier-based pwm schemes," *IEEE Transactions on Industry Applications*, vol. 32, no. 5, pp. 1122–1129, 1996.

[25] A. Trzynadlowski and S. Legowski, "Minimum-loss vector pwm strategy for three-phase inverters," *IEEE Transactions on Power Electronics*, vol. 9, no. 1, pp. 26–34, 1994.

[26] R. Peña-Alzola, M. Liserre, F. Blaabjerg, M. Ordonez, and Y. Yang, "Lcl filter design for robust active damping in grid-connected converters," *IEEE Transactions on Industrial Informatics*, vol. 10, no. 4, pp. 2192–2203, 2014.

[27] A. Reznik, M. G. Simões, A. Al-Durra, and S. M. Muyeen, "Lcl filter design and performance analysis for grid-interconnected systems," *IEEE Transactions on Industry Applications*, vol. 50, no. 2, pp. 1225–1232, 2014.

[28] T.-F. Wu, M. Misra, L.-C. Lin, and C.-W. Hsu, "An improved resonant frequency based systematic lcl filter design method for grid-connected inverter," *IEEE Transactions on Industrial Electronics*, vol. 64, no. 8, pp. 6412–6421, 2017.

[29] S. G. Parker, B. P. McGrath, and D. G. Holmes, "Regions of active damping control for lcl filters," in *2012 IEEE Energy Conversion Congress and Exposition (ECCE)*, pp. 53–60, 2012.

[30] Y. Tang, W. Yao, P. C. Loh, and F. Blaabjerg, "Design of lcl-filters with lcl resonance frequencies beyond the nyquist frequency for grid-connected inverters," in *2015 IEEE Energy Conversion Congress and Exposition (ECCE)*, pp. 5137–5144, 2015.

[31] Y. Tang, C. Yoon, R. Zhu, and F. Blaabjerg, "Generalized stability regions of current control for lcl-filtered grid-connected converters without passive or active damping," in *2015 IEEE Energy Conversion Congress and Exposition (ECCE)*, pp. 2040–2047, 2015.

[32] J. Wang, J. D. Yan, L. Jiang, and J. Zou, "Delay-dependent stability of single-loop controlled grid-connected inverters with ¡italic¿lcl¡/italic¿ filters," *IEEE Transactions on Power Electronics*, vol. 31, no. 1, pp. 743–757, 2016.

[33] M. Stecca, T. B. Soeiro, L. R. Elizondo, P. Bauer, and P. Palensky, "Comparison of two and three-level dc-ac converters for a 100 kw battery energy storage system," in *2020 IEEE 29th International Symposium on Industrial Electronics (ISIE)*, pp. 677–682, 2020.

Yang Wu (Student Member, IEEE) received the B.S. degree in electrical engineering and automation from Southeast University, Nanjing, China, in 2017 and the M.Sc. (cum laude) degree in electrical power engineering in 2019 from the Delft University of Technology, Delft, The Netherlands, where he is currently working toward the Ph.D. degree in electrical engineering from DCES Group (dc systems, energy conversion and storage)

His current research interests include the PWM and control strategies of the grid-connected converter for the EV fast charger.

Junzhong Xu (Member, IEEE) was born in Ningbo, China, in 1994. He received the B.S. degree in electrical engineering from Harbin Institute of Technology, Harbin, China, in 2016, and the Ph.D. degree in electrical engineering from Shanghai Jiao Tong University, Shanghai, China, in 2021.

From Jan. 2020 to Jun. 2021, he was a Visiting Scholar with the DC Systems, Energy Conversion and Storage Group, Delft University of Technology, Delft, The Netherlands. He is currently a Post-doctoral Research Fellow with the Department of Electrical Engineering, Shanghai Jiao Tong University, Shanghai, China. His research interests include advanced control and modulation for power converters.

Thiago Batista Soeiro (Senior Member, IEEE) received the B.S. (Hons.) and M.S. degrees in electrical engineering from the Federal University of Santa Catarina, Florianopolis, Brazil, in 2004 and 2007, respectively, and the Ph.D. degree from the Swiss Federal Institute of Technology, Zurich, Switzerland, in 2012.

During the masters and Ph.D. studies, he was a Visiting Scholar at the Power Electronics and Energy Research Group, Concordia University, Montreal, QC, Canada, and at the Center for Power Electronics Systems, Blacksburg, VA, USA, respectively. From 2012 to 2013, he was a Senior Engineer at the Power Electronics Institute, the Federal University of Santa Catarina. From 2013 to 2018, he was a Senior Scientist at the Corporate Research Center, ABB Switzerland Ltd. From 2018 to 2021, he was affiliated to the DC Systems, Energy Conversion and Storage Group, Delft University of Technology, Delft, The Netherlands, where he successfully acquired his Tenure academic position and worked as an Associate Professor for high power electronics. Since January 2022 he has been affiliated to the European Space Agency (ESA) at the European Space Research and Technology Centre (ESTEC) in Noordwijk, the Netherlands, where he works on the R&D of power conditioning and distribution units for satellites.

Marco Stecca (Student Member, IEEE) received the bachelor's degree in energy engineering from the University of Padova, Italy, in 2016, and the master degree in electrical engineering from Politecnico di Milano, Italy, in 2018. Since 2018 he has been working toward the Ph.D. degree in the field of grid scale battery energy storage systems with the Delft University of Technology.

His research interests include grid connected DC-AC power electronics converters and energy storage system integration in distribution grids.

Pavol Bauer (Senior Member, IEEE) is currently a full Professor with the Department of Electrical Sustainable Energy of Delft University of Technology and head of DC Systems, Energy Conversion and Storage group. He received Masters in Electrical Engineering at the Technical University of Kosice ('85), Ph.D. from Delft University of Technology ('95) and title prof. from the president of Czech Republic at the Brno University of Technology (2008) and Delft University of Technology (2016). He published over 72 journal and almost 300 conference papers in my field (with H factor Google scholar 43, Web of science 20), he is an author or co-author of 8 books, holds 4 international patents and organized several tutorials at the international conferences.

He has worked on many projects for industry concerning wind and wave energy, power electronic applications for power systems such as Smarttrafo; HVDC systems, projects for smart cities such as PV charging of electric vehicles, PV and storage integration, contactless charging; and he participated in several Leonardo da Vinci and H2020 EU projects as project partner (ELINA, INETELE, E-Pragmatic) and coordinator (PEMCWebLab.com-Edipe, SustEner, Eranet DCMICRO).